

## Article

# Robustness of Wireless Power Transfer Systems with Parity-Time Symmetry and Asymmetry

Haiyan Zhang<sup>1,†</sup>, Kejia Zhu<sup>2,†</sup>, Zhiwei Guo<sup>1</sup> , Yuguang Chen<sup>1</sup>, Yong Sun<sup>1</sup> , Jun Jiang<sup>3,4,\*</sup>, Yunhui Li<sup>1,2,\*</sup>, Zhuoping Yu<sup>4</sup> and Hong Chen<sup>1</sup>

<sup>1</sup> School of Physics Science and Engineering, Tongji University, Shanghai 200092, China; yongsun@tongji.edu.cn (Y.S.)

<sup>2</sup> Department of Electrical Engineering, Tongji University, Shanghai 201804, China

<sup>3</sup> Postdoctoral Station of Mechanical Engineering, Tongji University, Shanghai 200092, China

<sup>4</sup> College of Automotive Studies, Tongji University, Shanghai 201804, China

\* Correspondence: 503jiangjun@tongji.edu.cn (J.J.); liyunhui@tongji.edu.cn (Y.L.)

† These authors contributed equally to this work.

**Abstract:** Recently, wireless power transfer (WPT) technology has attracted much attention and shown rapid development. However, a fundamental challenge emerges in practical applications: how to achieve robust power transfer against the variation of operating conditions, such as the fluctuation of transfer distance, as well as the relative orientation of resonant coils. In this article, we theoretically propose and experimentally demonstrate that the robustness of a parity-time (PT) asymmetric system with unbalanced gain-loss working in a weak coupling region can be improved significantly, compared with that of a PT-symmetric system with balanced gain-loss working in a strong coupling region under the premise that the system works at a fixed optimal frequency. A pure real mode known as bound state in the continuum (BIC) in the weak coupling region of the PT-asymmetric system is adopted to ensure the high efficiency and stability of the WPT and break the limitations of balanced gain-loss of the PT-symmetric system. The better robustness performance originates from the orthogonal state with a pure real eigenmode embedded in the weak coupling region. Further experiments also verify that the PT-asymmetric system can achieve higher efficiency than that of the PT-symmetric system. In addition, we discuss the performance of the WPT system based on the theories of coupled mode theory (CMT) and circuit theory (CT); the BIC in the framework of CMT and a perfect impedance matching condition in the framework of CT for efficient power transfer are consistent. We also conducted power experimental verification of 30 watts, and found the efficiency between the coils can reach over 90% in dynamic scenarios, which meets expectations. The presented framework extends the field of non-Hermitian physics, bridges the gap between the non-ideal PT-symmetric system and a practical engineering application, and introduces a novel WPT mechanism for flexible application scenarios. Our results could provide instructive significance for practical applications of the WPT system in the long term.

**Keywords:** non-Hermitian physics; bound state in the continuum; wireless power transfer; robustness



**Citation:** Zhang, H.; Zhu, K.; Guo, Z.; Chen, Y.; Sun, Y.; Jiang, J.; Li, Y.; Yu, Z.; Chen, H. Robustness of Wireless Power Transfer Systems with Parity-Time Symmetry and Asymmetry. *Energies* **2023**, *16*, 4605. <https://doi.org/10.3390/en16124605>

Academic Editors: Mauro Feliziani and Byoung Kuk Lee

Received: 10 April 2023

Revised: 3 June 2023

Accepted: 7 June 2023

Published: 8 June 2023



**Copyright:** © 2023 by the authors. Licensee MDPI, Basel, Switzerland. This article is an open access article distributed under the terms and conditions of the Creative Commons Attribution (CC BY) license (<https://creativecommons.org/licenses/by/4.0/>).

## 1. Introduction

Parity-time (PT) symmetry originated in quantum mechanics [1], which laid a solid foundation for applications in various fields. A significant amount of work based on PT symmetry has appeared in various fields, including quantum and atomic [2,3] systems, metamaterials [4,5], acoustic [6–9], and electronics [10,11]. Simultaneously, researchers have observed many novel phenomena based on PT symmetry, such as wireless power transfer (WPT) [12–15], energy level attraction [16], unidirectional invisibility [17], non-reciprocal light transmission [18–21], PT-symmetric lasers [22–24], coherent perfect absorber [25], wireless sensor [26,27], etc. In particular, PT-symmetric systems exhibit symmetry breaking near the exceptional point (EP), and the eigenvalue undergoes evolution from real to

complex [9,28–32], with many counterintuitive phenomena and applications based on EP, including ultra-sensitive wireless sensors [26], directional lasing [33] and chirality [34]. It is generally believed that the optimal operating mode of a second-order magnetic resonant WPT system exists in the strong coupling regime by maintaining PT symmetry or at the exceptional point (EP), where pure real eigenvalues are always implemented. However, the scheme faces the disadvantage of tracking the optimal operating frequency when the coupling strength between the coupled resonators changes, such as for mobile receivers. In addition, due to the strict conditions of PT symmetry, it is difficult to generalize to higher-order systems and power multiple loads without sacrificing efficiency.

In the early 20th century, much effort was devoted to the development of schemes to transfer energy over long distances without any carrier medium; this was explored by Nikola Tesla experimentally [35] and the breakthrough has greatly compensated for traditional wired cables. In 2007, a research group at MIT successfully achieved a result with around 60 watts of power transferred with an efficiency of about 40% over a distance of more than 2 m by magnetic resonant coupling, where the diameter of the two resonant coils is 60 cm [36]. Undoubtedly, the WPT technique has shown great commercial potential due to its advantages of safety and convenience, especially in a scenario where it is not convenient to supply power to electrical appliances through wired cables. Currently, with the development of WPT-related theories and the improvement of hardware facilities, WPT technology is being intensively explored to apply in various applications, such as consumer electronics [37,38], implantable medical devices [39–42] and electric vehicle charging [43], etc.

In practical terms, wireless power transfer with high efficiency and stability is required for a WPT system, which is an important foundation for its widespread applications. However, since the application scenario is always variable, a stable and efficient power transfer efficiency against the variation of operating conditions is exactly what we desire, and many methods have been put forward simultaneously. Typically, in order to achieve efficient wireless power transfer by amplifying the near-field, suitable metamaterials [44–47] or metasurfaces [48] must be designed and used. Recently, applying a high-Q quasi-MDBIC of all-dielectric metasurface to achieve efficient and robust WPT was realized [49], due to the fact that metasurfaces can greatly enhance magnetic resonance. Furthermore, a nonlinear parity-time symmetric circuit was proposed to achieve efficient and robust wireless power transfer over a distance variation of approximately one meter, without the need for any tuning [12], which is of benefit to charging moving devices or vehicles. In addition, with high-order PT symmetry, efficient WPT can be achieved without frequency tracking at varying distances [14], and it can also be applied for powering miniaturized receivers and multiple loads. Recently, anapole-based ultracompact and high-efficiency electromagnetic energy transfer has also emerged [50].

Generally speaking, two different theories can be used to analyze the power transfer performance of the WPT systems, that is, the coupled mode theory (CMT) which describes energy distribution of coupled resonators, and the classical circuit theory (CT) which describes the voltage and current distributions of circuit topology. In addition, CMT is an approximation method under the condition of a small coupling coefficient and high-quality factor. On the contrary, CT is more accurate than CMT for WPT systems but ignores the gain and loss rates of the resonators. The two theories have their respective merits, but there is a certain degree of unity.

In this article, we design two types of magnetic coupling WPT systems, including the PT-symmetric system and the PT-asymmetric system. We further compare the robustness of the PT-symmetric system working in the strong coupling region with the PT-asymmetric system working in the weak coupling region. As a result, we find that the stability of the latter is significantly better than that of the former under the premise that the system works at a fixed optimal frequency, which we verify experimentally. In the meantime, we prove that the orthogonal state contributes to better robust performance. In addition, we find that the PT-asymmetric system can achieve a higher efficiency than that of the PT-symmetric system, without the need for complex circuit design [12].

The novelty of our work is that it achieves efficient and stable wireless power transfer with the help of the BIC mode hidden in the weak coupling region of the PT-asymmetric systems, which breaks the strict limitations of PT symmetry with balanced gain and loss, expands the application of non-Hermitian physics, and paves the way toward efficient and stable wireless power transfer systems that could be used in a multitude of applications, such as wireless charging of electric vehicles and implantable medical devices.

Section 1 reviewed the application of PT symmetry in various fields and the development of the WPT system design briefly, and the remainder of this paper is arranged as follows. In Section 2, the theoretical analysis is demonstrated based on the CMT and CT models, and the experimental results are verified based on the system prototype. Section 3 states the robustness of working in the strong coupling region of the PT-symmetric system and the weak coupling region of the PT-asymmetric system. Finally, Section 4 concludes the paper.

## 2. Theoretical Analysis and Experimental Verification

Here, we consider the second-order PT-symmetric and PT-asymmetric WPT systems, including two resonant coils strongly coupled together through near-field electromagnetic interaction, where one of them receives energy input (emitter) and the other supplies energy to the load (receiver); schematic diagrams of such systems are shown in Figure 1a,b. All coils are arranged coaxially, with an outer radius of  $R = 10$  cm. We compare the robustness of the PT-symmetric system working in the strong coupling region with the PT-asymmetric system working in the weak coupling region. The excitation source is set to be a continuous harmonic input with frequency  $\omega$ ,  $s_{1+} = S_{1+}e^{-i\omega t}$ , and the system dynamics can be described by the coupled mode equations as follows:

$$\frac{da_1}{dt} = (-i\omega_0 - \gamma_1 - \Gamma_1)a_1 - i\kappa a_2 + \sqrt{2\gamma_1}s_{1+}, \quad (1)$$

$$\frac{da_2}{dt} = (-i\omega_0 - \gamma_2 - \Gamma_2)a_2 - i\kappa a_1. \quad (2)$$

Here,  $a_{1,2} = A_{1,2}e^{-i\omega t}$  indicates the resonance modes of the transmitter coil and the receiver coil, where  $|a_1|^2$  and  $|a_2|^2$  represent the energy stored in the resonant coils.  $\omega_0$  and  $\Gamma_{1,2}$  are the resonant frequency and the intrinsic dissipative loss of the two resonant coils, respectively, and  $\kappa$  represents the coupling strength, which is related to axial transfer distance and lateral misalignment between the resonant coils.  $\gamma_1$  and  $\gamma_2$  represent the coupling rate between the source (or load) coil and the transmitter (or receiver) coil, which is related to the distance  $d_1$  (or  $d_2$ ).

According to the method in [14,25,51,52], when the system has no reflection,  $s_{1-} = -s_{1+} + \sqrt{2\gamma_1}a_1 = 0$ , it can be equivalent to a closed system. At this time, we can get

$$\mathbf{H} \begin{pmatrix} a_1 \\ a_2 \end{pmatrix} = \omega \begin{pmatrix} a_1 \\ a_2 \end{pmatrix}, \quad (3)$$

where the effective Hamiltonian is

$$\mathbf{H} = \begin{pmatrix} \omega_0 + i\gamma_1 - i\Gamma_1 & \kappa \\ \kappa & \omega_0 - i\gamma_2 - i\Gamma_2 \end{pmatrix}, \quad (4)$$

by solving the characteristic equation  $|\omega\mathbf{I} - \mathbf{H}| = 0$  (where  $\mathbf{I}$  is an identity matrix), the eigenfrequencies of the system are

$$\omega_{\pm} = \omega_0 + i \frac{(\gamma_1 - \Gamma_1) - (\gamma_2 + \Gamma_2)}{2} \pm \sqrt{\kappa^2 - \left( \frac{(\gamma_1 - \Gamma_1) + (\gamma_2 + \Gamma_2)}{2} \right)^2}. \quad (5)$$

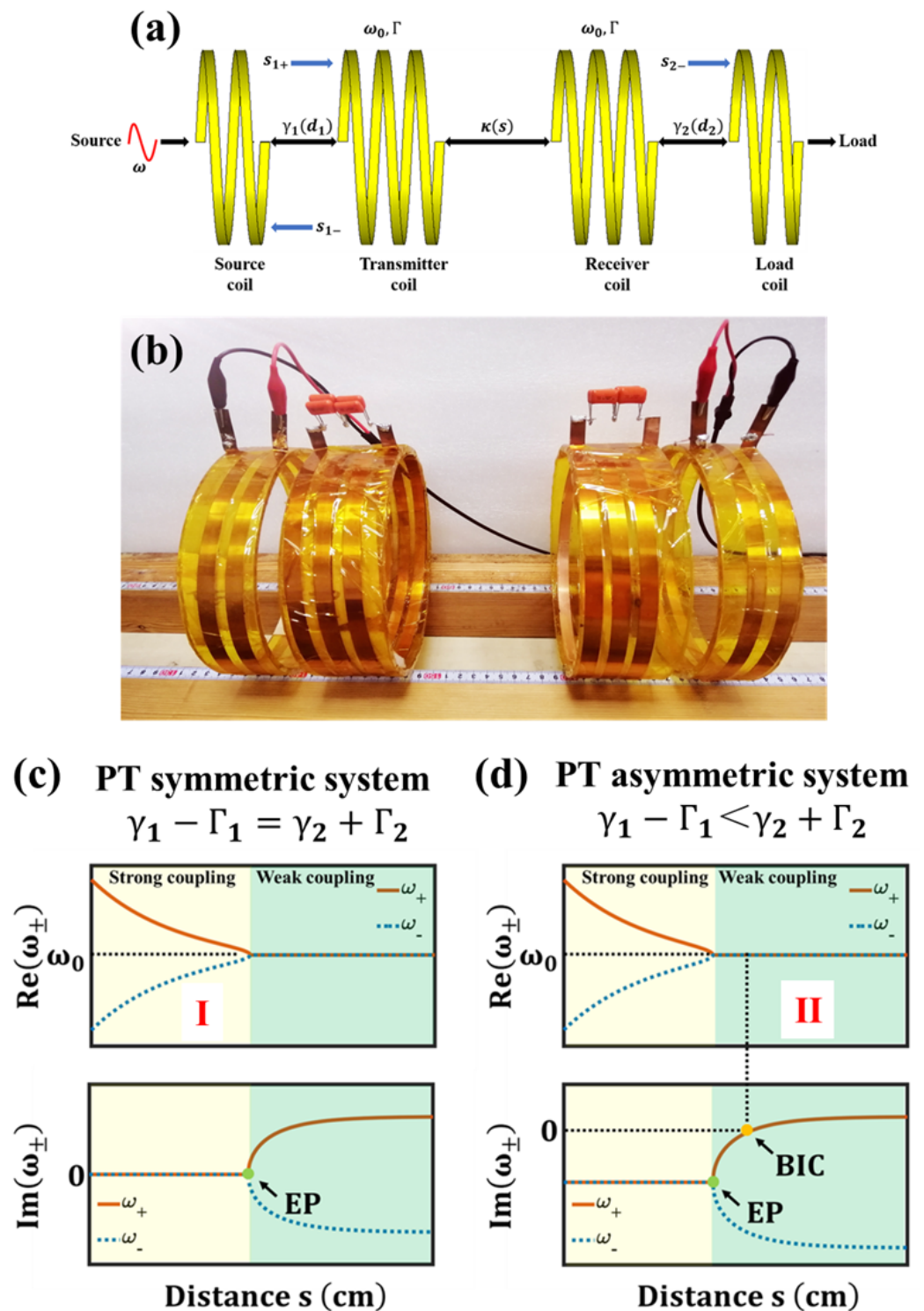


**Figure 1.** WPT system and eigenmode analysis. (a) Schematic of the WPT system. The excitation source is a continuous harmonic wave at a frequency  $\omega$ , which is coupled to the transmitter coil at the gain rate  $\gamma_1(d_1)$ , and the energy is transferred through the receiver coil, and then output to the load coil at the loss rate  $\gamma_2(d_2)$ . Transmitter–receiver resonant coupling rate is  $\kappa$ , which varies as a function of transfer distance and the relative orientation of the resonant coils. (b) Photograph of the WPT system, which corresponds to (a). (c) Real ( $\text{Re}(\omega_{\pm})$ ) and imaginary ( $\text{Im}(\omega_{\pm})$ ) eigenfrequencies of the PT–symmetric system. (d) Real ( $\text{Re}(\omega_{\pm})$ ) and imaginary ( $\text{Im}(\omega_{\pm})$ ) eigenfrequencies of the PT–asymmetric system.

As for the PT-symmetric system,  $\gamma_1 - \Gamma_1 = \gamma_2 + \Gamma_2$ , efficient wireless power transfer can be achieved in the strong coupling region, which has a real eigenvalue, as shown in area I of Figure 1c. However, as for the PT-asymmetric system, it can enter the weak coupling region to ensure that it resonates at a fixed working frequency  $\omega_0$  as shown in area II of Figure 1d, and support maximized efficiency at one point called BIC,  $\kappa^2 = (\gamma_1 - \Gamma_1)(\gamma_2 + \Gamma_2)$ , which corresponds to a pure real mode. Theoretically, the power transfer efficiency can approach near unity upon reaching resonance at the mode of BIC, where the resonators are reflectionless. The BIC condition corresponds perfectly to the zero reflection condition, which is also an important building block for efficient power transfer.

Then, the transfer efficiency of the dual-resonator WPT system is analyzed. Substituting  $a_{1,2} = A_{1,2}e^{-i\omega t}$  into Equations (1) and (2), at the steady state ( $\frac{dA_{1,2}}{dt} = 0$ ), the amplitudes of the two resonant coils are

$$A_1 = \frac{-\sqrt{2(\gamma_1 + \Gamma_1)}[i(\omega - \omega_0) - (\gamma_2 + \Gamma_2)]S_{1+}}{\kappa^2 + [i(\omega - \omega_0) - (\gamma_1 + \Gamma_1)][i(\omega - \omega_0) - (\gamma_2 + \Gamma_2)]} \quad (6)$$

$$A_2 = \frac{-\sqrt{2(\gamma_1 + \Gamma_1)}[i(\omega - \omega_0) - (\gamma_2 + \Gamma_2)]S_{1+}}{\kappa^2 + [i(\omega - \omega_0) - (\gamma_1 + \Gamma_1)][i(\omega - \omega_0) - (\gamma_2 + \Gamma_2)]} \quad (7)$$

The reflection  $S_{1-}$  and transmission  $S_{2-}$  for the system are given as  $S_{1-} = -S_{1+} + \sqrt{2\gamma_1}A_1$  and  $S_{2-} = \sqrt{2\gamma_2}A_2$ , respectively. Therefore, the wireless power transfer efficiency of such a dual-resonator WPT system can be obtained in an open system format

$$\eta = \left| \frac{s_{2-}}{s_{1+}} \right|^2 = \left| \frac{2\sqrt{\gamma_1\gamma_2}\kappa(s)}{\kappa(s)^2 + [i(\omega - \omega_0) - (\gamma_1 + \Gamma_1)][i(\omega - \omega_0) - (\gamma_2 + \Gamma_2)]} \right|^2. \quad (8)$$

At the present time, an efficient and robust WPT system, which can be applied to dynamic wireless charging scenarios, such as powering traveling electric vehicles, is greatly desired. Here, taking the practical application into account, based on Equation (8), what we mainly analyze is the stability of the WPT system against the variation of operating conditions, such as the transfer distance, as well as the relative orientation of the two resonant coils.

In this work, all coils are made of the copper sheet with a width of 1 mm and a thickness of 0.3 mm and attached tightly to the poly(methyl methacrylate) (PMMA) hollow circular cylinder with an outer radius of  $R = 10$  cm. The source coil, transmitting coil and receiving coil are respectively made of two-turn and three-turn copper strips, and the load coil is made of two-turn (area I in Figure 1c) or nine-turn (area II in Figure 1d) copper strip. In addition, the capacitance  $C = 2.02$  nF is made up of a lumped-metallized polyester film capacitor (withstand voltage more than 2000 V). The four coils are arranged on a wooden rod and are able to slide coaxially. All relevant electrical parameters are measured by using the precision LCR digital bridge (AT2818, Applient) as follows:  $L \approx 2.97$   $\mu$ H,  $C \approx 2.02$  nF, and each resonant coil is tuned at a frequency of 2.055 MHz, which has a measured intrinsic quality factor of  $Q = 406$ . The information provided by the WPT system is then read by a-R and R terms connected to Port 1 and Port 2 of the vector network analyzer (Keysight E5071C, the source impedance is 50  $\Omega$ ), respectively. For measuring the transmission ( $S_{21}$ ) spectra, where  $\eta = |S_{21}|^2$  represents the power transfer efficiency, both theoretical calculation and experimental results are based on the fixed parameters of  $\omega_0 = 2.055$  MHz,  $\gamma_1 = 0.0561951$  MHz and  $\Gamma_1 = \Gamma_2 = 0.0048804$  MHz. The case of balanced gain and loss corresponds to the PT-symmetric system, while the case of unbalanced gain and loss corresponds to the PT-asymmetric system. The gain rate and loss rate are adjusted by the distance between the non-resonant coil and the resonant coil in the experiment. In addition, one reason for choosing this operating frequency is that compared to higher frequencies, our designed operating frequency is more suitable for commercial applications, saving

hardware facility costs, such as MOSFETs. The frequency of around 2 MHz reaches the upper limit of SiC devices, which is also suitable for the structural dimensions of this article.

The above is an analysis of the conditions for achieving efficient power transfer in WPT systems derived from the CMT model. Moreover, the system in Figure 1a can be described by the CT model. As shown in Figure 2, when the resistance of electronic components is ignored, using Kirchoff’s laws, the voltages and currents are related as

$$\begin{pmatrix} i\omega L + \frac{1}{i\omega C} - R_s & -i\omega mL \\ -i\omega mL & i\omega L + \frac{1}{i\omega C} + R_L \end{pmatrix} \begin{pmatrix} I_1 \\ I_2 \end{pmatrix} = \begin{pmatrix} 0 \\ 0 \end{pmatrix}, \tag{9}$$

where  $C$  is the lumped capacitance and  $L$  is the distributed inductance of the coil.  $R_s$  and  $R_L$  are source impedance and load impedance, respectively.  $M$  is the mutual inductance between the two resonant coils,  $M = mL$ , where  $m$  represents the coupling coefficient between the two coils.  $U = -I_1R$  is the AC source.

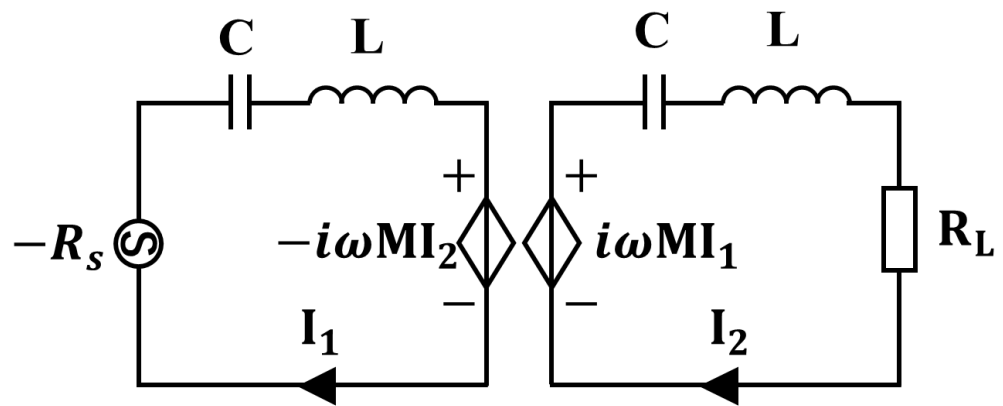


**Figure 2.** The equivalent circuit schematic diagram of the wireless power transfer system corresponding to Figure 1a.

In Equation (9), when we take the derivative of current with respect to time, combine  $a_n = L_n \frac{dI_n}{dt} = -i\omega L_n \frac{dI_n}{dt}$  ( $n = 1, 2$ ) and utilize the approximate condition  $\omega^2 - \omega_0^2 \approx 2\omega(\omega - \omega_0)$ , Equation (9) is denoted as

$$\begin{pmatrix} \omega - \omega_0 + \frac{iR_s}{2L} & -\frac{\omega_0 m}{2} \\ -\frac{\omega_0 m}{2} & \omega - \omega_0 - \frac{iR_L}{2L} \end{pmatrix} \begin{pmatrix} a_1 \\ a_2 \end{pmatrix} = \begin{pmatrix} 0 \\ 0 \end{pmatrix}, \tag{10}$$

where  $\omega_0$  is the resonant frequency, that is,  $\omega_0 = 1/\sqrt{LC}$ . Equation (10) can be regarded as the coupled mode equation describing the second-order system where  $a_n = A_n e^{-i\omega t}$  ( $n = 1, 2$ ), and the case of  $R_s = R_L$  corresponds to the ideal PT-symmetric system. By comparing Equation (10) with Equations (3) and (4), the relationships between gain, loss, coupling strength and circuit parameters (RLC) are expressed as  $\gamma_1 = \frac{R_s}{2L}$ ,  $\gamma_2 = \frac{R_L}{2L}$  and  $\kappa = -\frac{\omega_0 m}{2}$  in the lossless WPT system. Therefore, the BIC condition  $\kappa^2 = \gamma_1 \gamma_2$  is also equivalent to  $m^2 = \frac{R_s R_L C}{L}$ .

Then the reflected impedance  $Z_{ref}$  and the input impedance  $Z_{in}$  of the WPT system can be deduced as follows [53]:

$$Z_{ref} = \frac{-i\omega MI_2}{I_1}, \tag{11}$$

According to the second closed circuit, based on Kirchoff’s laws, we get

$$i\omega MI_1 = I_2 \left( \frac{1}{i\omega C} + i\omega L + R_L \right) \tag{12}$$

Therefore, the reflected impedance and the input impedance are deduced as

$$Z_{ref} = \frac{\omega^2 M^2}{\frac{1}{i\omega C} + i\omega L + R_L} \quad (13)$$

$$Z_{in} = Z_{ref} + \frac{1}{i\omega C} + i\omega L \quad (14)$$

Then we can analyze the relationships between the real and imaginary parts of the input impedance with frequency. As shown in Figure 3a, the imaginary part of the input impedance is exactly 0 at the resonant frequency of the system, that is, the system presents pure resistance. We also notice that the real part of the input impedance at this time is 50 ohm, as shown in Figure 3b, that is, the impedance of the whole system and the input source perfectly matches, thus realizing efficient and stable wireless power transfer. The impedance matching process is self-consistent with the results of wireless power transfer of pure real mode BIC analyzed in the previous paper.

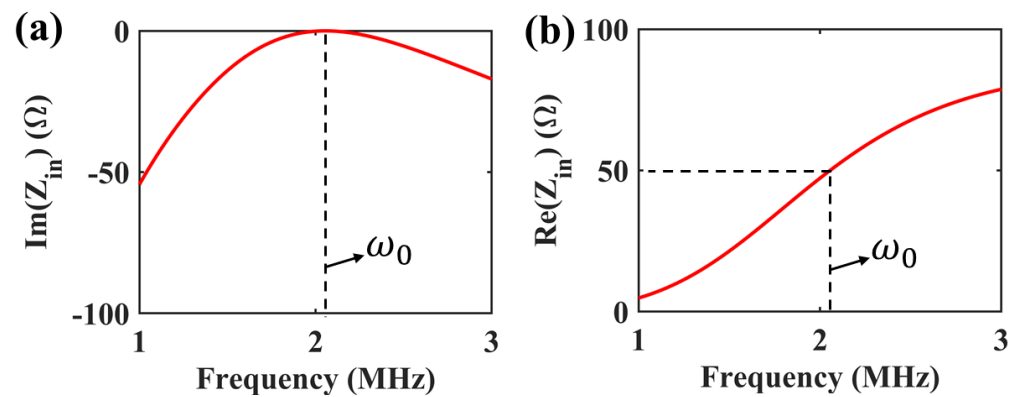


**Figure 3.** Analysis of (a) real and (b) imaginary parts of input impedance under the condition of  $m^2 = \frac{R_s R_L C}{L}$  derived from the CMT model.

### 3. Robustness Analysis

Taking the perturbation of the transfer distance as an example, Figure 4a,c shows the WPT efficiency spectra. Figure 4b,d shows that the transfer efficiency versus transfer distance corresponds to three different coupling strengths in areas I and II, respectively, which satisfies  $\kappa(s_1) > \kappa(s_2) > \kappa(s_3)$ .

First, for a fixed transfer distance, by adjusting the loss rate  $\gamma_2$ , the system changes from the strong coupling region in the PT-symmetric system (area I in Figure 1c) to the weak coupling region in the PT-asymmetric system (area II in Figure 1d) in order to work. When the distance changes by 5 cm around  $s_1 = 1$  cm, the efficiency drops  $\Delta\eta_{1\text{ cm} \rightarrow 6\text{ cm, area I}} = 79.36\%$  (dark blue line in Figure 4b) and  $\Delta\eta_{1\text{ cm} \rightarrow 6\text{ cm, area II}} = 38.81\%$  (yellow line in Figure 4d), respectively. In the same way, we get the results of  $\Delta\eta_{5\text{ cm} \rightarrow 10\text{ cm, area I}} = 63.74\%$  (orange line in Figure 4b),  $\Delta\eta_{5\text{ cm} \rightarrow 10\text{ cm, area II}} = 39.09\%$  (purple line in Figure 4d), as well as  $\Delta\eta_{10\text{ cm} \rightarrow 15\text{ cm, area I}} = 44.38\%$  (green line in Figure 4b),  $\Delta\eta_{10\text{ cm} \rightarrow 15\text{ cm, area II}} = 39.47\%$  (light blue line in Figure 4d). Above all, compared with the PT-symmetric system working in the strong coupling region, Figure 4b,d clearly shows that the PT-asymmetric system working in the weak coupling region is more robust compared with the change in distance.

Further, we find that the greater the coupling strength, the faster the transfer efficiency drops compared with the change in the distance when working in area I of Figure 1c. However, the efficiency drops at almost the same rate to the change in distance at three different coupling strengths when working in area II of Figure 1d, where the efficiency decay rate is hardly affected by the coupling strength.

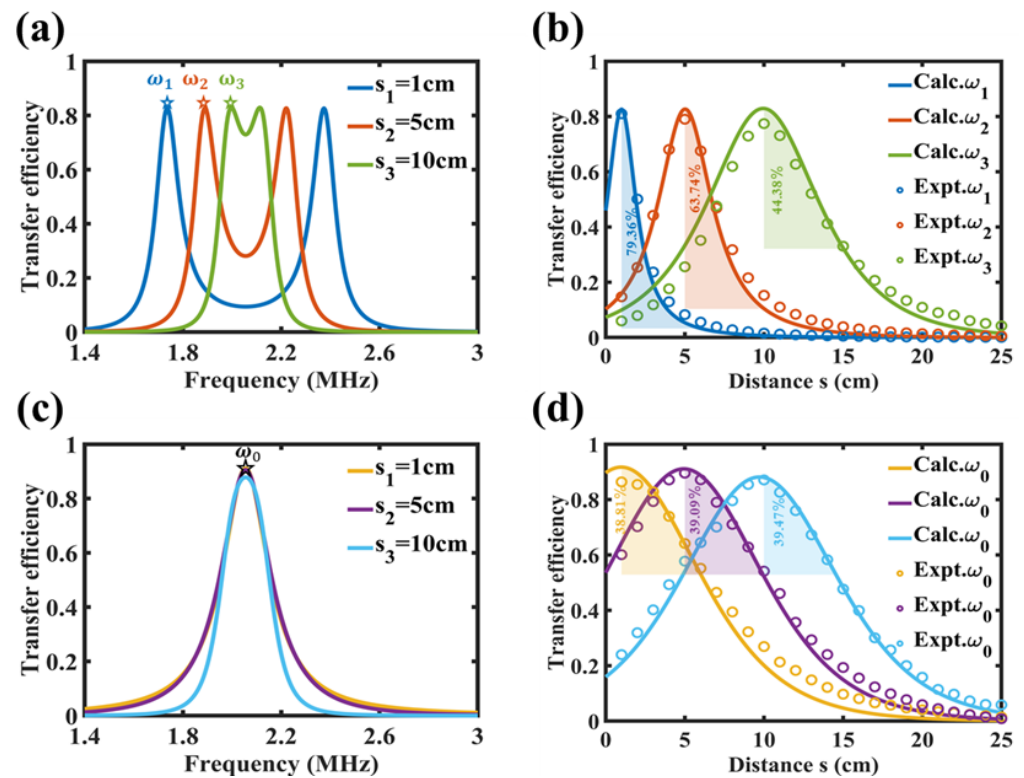


**Figure 4.** Robustness analysis of the WPT system with the measurement results of network analyzer. (a) Spectra corresponding to three different coupling strengths in the strong coupling region of the PT-symmetric system. (b) Evolution of the transfer efficiency with the distance corresponding to (a). (c) Spectra corresponding to three different coupling strengths in the weak coupling region of the PT-asymmetric system. (d) Evolution of the transfer efficiency with the distance corresponding to (c). The solid line is the theoretical results corresponding to Equation (5), the hollow circles are the experimental results, and the experimental results are in good agreement with the theoretical ones obtained by coupled mode theory.

Considering practical applications, we conduct a new experiment and measure the overall efficiency of the system in the case of considering conduction and switching losses in power converters, and the corresponding experimental diagram and results are presented in Figure 5. Here, we use a full-bridge inverter circuit as the AC source is about 90% efficient. Furthermore, a full-bridge rectifier circuit with an efficiency of about 92%, is used at the front end of the load. Due to the short preparation time of the experiments, MOSFETs and diodes in the power convector circuits use silicon substrate which is more suitable for low-frequency systems, so the efficiency is not as high as SiC or GaN-based devices. The experimental results are in good agreement with the theoretical values, and there is a certain deviation due to factors such as losses introduced by high-frequency power convector circuits. In addition, the input power of the DC power supply is carefully controlled at 30~31 watts to ensure the fairness of all experimental data. In real-world scenarios, DC-DC conversion circuits such as BUCK and phase-shift full-bridge can be used to control gain/loss intensity, so as to automatically track BIC conditions in the PT-asymmetry WPT system.

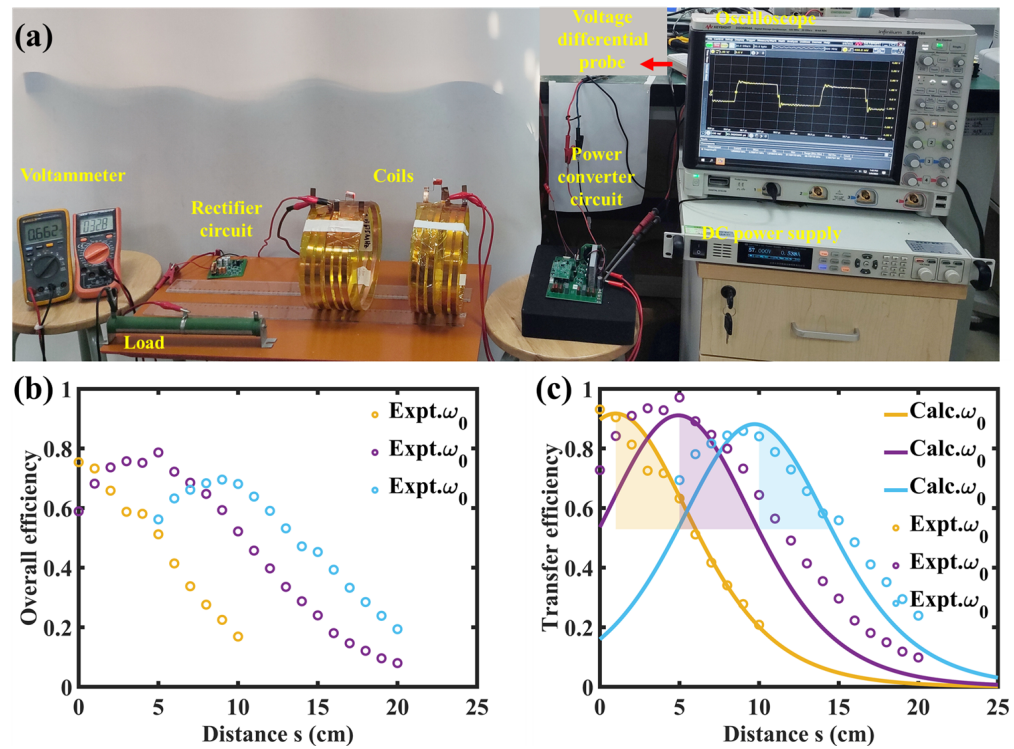


**Figure 5.** Transfer performance of the WPT system when the transmitting end is loaded with 30 W power. (a) Photo of the experimental prototype. The evolution of (b) the overall efficiency and (c) the transfer efficiency, with the distance corresponding to the same parameters as Figure 4d.

Simultaneously, as shown in Figure 6a, it is obvious that the PT-asymmetric system keeps higher efficiency and better robustness at the fixed optimal frequency  $\omega_0$  than that of the PT-symmetric system at the varying optimal frequency  $\omega_{\pm}$  against the varying distance. Further, the excellent performance of wireless power transfer in the BIC scheme is remarkable at both varying non-axial offset distance  $h$  and varying offset angle  $\alpha$ , as shown in Figure 6b,c.

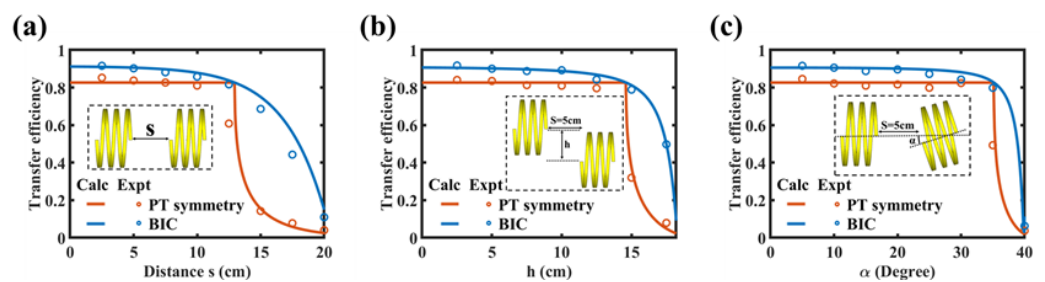


**Figure 6.** Comparison of optimal transfer efficiency. (a) The calculated transfer efficiency as a function of the separation distance  $s$  between the resonators for a frequency tracking ( $\omega_{\pm}$ ) scheme in the PT-symmetric system (orange line) and a BIC scheme with a fixed optimal frequency ( $\omega_0$ ) in the PT-asymmetric system (blue line). (b) The calculated transfer efficiency as a function of the non-axial offset distance  $h$  when  $s = 5$  cm. (c) The calculated transfer efficiency as a function of the offset angle  $\alpha$  when  $s = 5$  cm.

The phase difference between the two resonant coils is given as follows:

$$\Delta\varphi = \varphi_2 - \varphi_1 = \arccos\left(\frac{A_1}{|A_1|} / \frac{A_2}{|A_2|}\right) = \arccos\left(\frac{\pm\sqrt{\kappa^2 - \left[\frac{(\gamma_1 - \Gamma_1) + (\gamma_2 + \Gamma_2)}{2}\right]^2}}{\sqrt{\kappa^2 + (\gamma_2 + \Gamma_2)^2}}\right), \quad (15)$$

Based on Equation (7), when the system satisfies the PT-symmetric condition,  $\gamma_1 - \Gamma_1 = \gamma_2 + \Gamma_2$ , we get the diagram of phase difference, as shown in Figure 7a. In addition, the diagram of phase difference in the PT-asymmetric system  $\gamma_1 - \Gamma_1 < \gamma_2 + \Gamma_2$ , is plotted in Figure 7b.

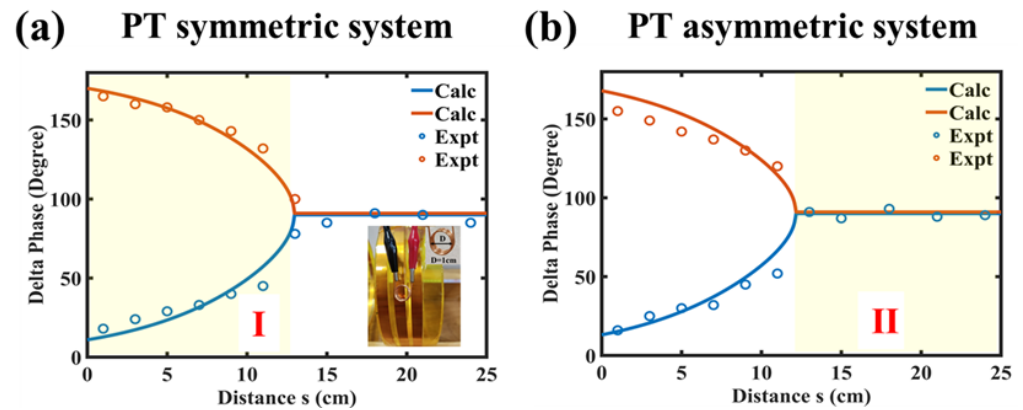


**Figure 7.** The evolution relationship of the phase difference between the transmitter-receiver resonant coils with the transfer distance in (a) the PT-symmetric system and (b) the PT-asymmetric system, respectively. The solid line represents the theoretical results obtained from Equation (6), and the hollow circles are the experimental results. In the experiment, a ring-shaped high-impedance probe with a diameter of 1 cm made of copper is close to the resonant coils with insulating tape to measure the phase of the resonators, as shown in the illustration of Figure 7a. Here area I and area II correspond to those in Figure 1c,d.

Figure 7a,b clearly shows that the phase difference between the two resonators is 90 degrees in the weak coupling region of the PT-asymmetric system (area II in Figure 7b), indicating that the system is in an orthogonal state. However, the two eigenmodes of the PT-symmetric system working in the strong coupling region (area I in Figure 7a) are not orthogonal. Therefore, it is actually the orthogonal state that guarantees that the system reaches a steady state rapidly against perturbation of distance, and this means the robustness of the PT-asymmetric system working in the weak coupling region is better.

In addition to the variation of the transfer distance of the two resonant coils we analyzed above, the relative orientation of the two resonant coils is also an important factor affecting the coupling strength. Specifically, the changes of coupling rates with these position parameters are plotted in Figure 8a–c.

The above three degrees of freedom (the transfer distance, the relative orientation including relative angle and relative height) essentially affect the coupling strength between the coupled resonators. Therefore, we can refer to the BIC condition to adjust the gain rate  $\gamma_1$  of the transmitter end or the loss rate  $\gamma_2$  of the receiver end, thereby achieving efficient and robust wireless power transfer, due to the fact that there is no strict restriction on balanced gain rate and loss rate in PT-asymmetric system. Therefore, based on the PT-asymmetric principle, the regulation method of stable and efficient working mode is relatively flexible, therefore, it can be applied to a wide range of wireless charging scenarios without being affected by operating environments and conditions. In all cases, we maintain a maximized total efficiency across various power transfer scenarios by simply tuning at each receiver end or transmitter end. Additionally, Figure 8d shows the gain rate  $\gamma_1$  varying with distance  $d_1$ , and the relationship between loss rate and distance  $\gamma_1(d_1)$  is the same as  $\gamma_2(d_2)$ , which guides us on how to adjust and implement BIC mode accompanied by efficient wireless power transfer in experiments.

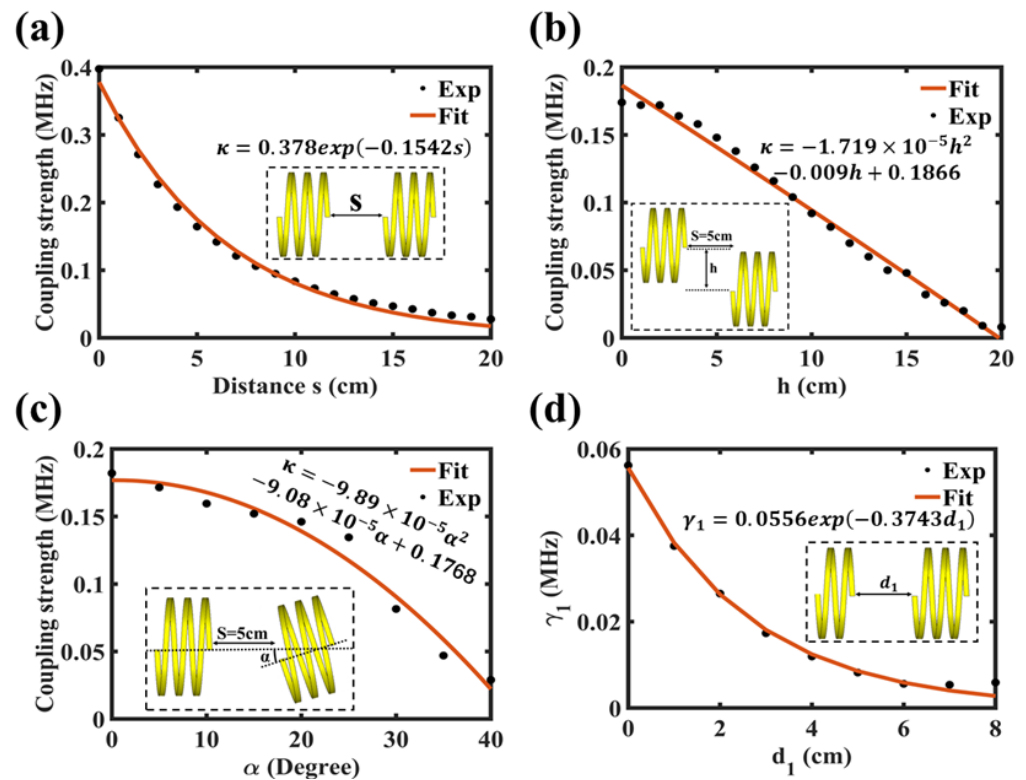


**Figure 8.** Coupling rates as a function of separation distance corresponding to Figure 1a. (a) Coupling rates between transmitter and receiver coils as a function of transfer distance  $s$  ( $\kappa(s)$ ). The transmission distance  $s$  is fixed at 10 cm. The fitting result is  $\kappa = 0.378\exp(-0.1542s)$ . (b) Coupling rates as a function of lateral offset distance  $h$  ( $\kappa(h)$ ) when transfer distance  $s$  is fixed at 5 cm. The fitting result is  $\kappa = -1.719 \times 10^{-5}h^2 - 0.009h + 0.1866$ . (c) Coupling rates as a function of offset angle  $\alpha$  ( $\kappa(\alpha)$ ) when transfer distance  $s$  is fixed at 5 cm. The fitting result is  $\kappa = -9.89 \times 10^{-5}\alpha^2 - 9.08 \times 10^{-5}\alpha + 0.1768$ . (d) Coupling rates between source and transmitter coils as a function of separation distance  $d_1$  ( $\gamma_1(d_1)$ ). Fitting result is  $\gamma_1 = 0.0556\exp(-0.3743d_1)$ .

#### 4. Conclusions

In conclusion, we propose a new scheme implementing efficient and robust wireless power transfer by accessing the BIC mode hidden in the weak coupling regime of the PT-asymmetric system. Specifically, the transfer efficiency of up to 80% is realized at a transfer distance of 10 cm in the experiment of loading power with the aid of BIC mode, where the radius of the resonance coils in the system is 10 cm. Furthermore, we have analyzed and compared the stability of the PT-symmetric system working in the strong coupling region and the PT-asymmetric system working in the weak coupling region both at a fixed optimal operating frequency. The results show that the efficiency of the PT-asymmetric system working in the weak coupling region is less sensitive to the position-dependent coupling strength, so it is more immune to perturbations such as fluctuation of the transfer distance, as well as the relative orientation of the resonant coils, corresponding to the change of coupling strength substantially, and this can be precisely attributed to the fact that the system in the weak coupling region is a self-orthogonal state. Moreover, compared with the PT-symmetric system, the PT-asymmetric system can achieve higher efficiency.

From this point of view, a PT-asymmetric WPT system working in the weak coupling region may be relatively more suitable for implementing a powerful WPT platform over a wide distance range without changing the operating frequency. In general, our results have certain guiding significance for the optimal working conditions of the WPT system. Moreover, our results could be extended to other physical platforms such as non-radiative acoustic wireless power transfer. In addition, the intrinsic physical properties and excellent performance of the orthogonal state are worthy of further exploration.

Importantly, we find that the pure real mode known as BIC of the system based on CMT and the impedance perfect matching based on CT are consistent, which corresponds to the mode of efficient wireless power transfer. Both CMT and CT have their own advantages and disadvantages; the former focuses on the energy distribution of the coupled resonators, while the latter focuses on circuit parameters. We can make appropriate choices based on specific requirements. Our work provides a new perspective for a deeper understanding of the WPT system through CMT or CT.

Last but not least, the implementation of pure real mode known as BIC lays the foundation for efficient WPT through gain or loss modulation and has the potential to be applied to third-order or even higher-order WPT systems to achieve efficient power supply for multiple loads. However, it is noteworthy that the transfer efficiency cannot reach the theoretical unit of 1 due to the influence of intrinsic losses such as internal resistance of components, and can only be reduced as much as possible in experiments by selecting high-quality electronic devices.

**Author Contributions:** Theoretical analysis, H.Z.; experiment, H.Z.; writing—original draft preparation, H.Z.; writing—review and editing, K.Z., Z.G., Y.C., Y.S., J.J. and Y.L.; supervision, Z.Y. and H.C. All authors have read and agreed to the published version of the manuscript.

**Funding:** This work was supported by the National Key R&D Program of China (Grant No. 2021YFA1400602), the National Natural Science Foundation of China (NSFC; Grant Nos. 12074286, 12004284, 12104342), the Shanghai Municipal Science and Technology Major Project (2021SHZDZX0100), and the Fundamental Research Funds for the Central Universities (Grant No. 22120210579), the Shanghai Science and Technology Innovation Action Plan Project “Research and Development of Automotive High-performance and Highly Integrated Motor Drive Transmission Assembly” (Grant No. 20511104602).

**Data Availability Statement:** The data presented in this study are available on request from the corresponding author.

**Conflicts of Interest:** The authors declare no conflict of interest.

## References

1. Bender, C.M.; Boettcher, S.; Meisinger, P.N. PT-symmetric quantum mechanics. *J. Math. Phys.* **1999**, *40*, 2201–2229. [[CrossRef](#)]
2. Peng, P.; Cao, W.; Shen, C.; Qu, W.; Wen, J.; Jiang, L.; Xiao, Y. Anti-parity–time symmetry with flying atoms. *Nat. Phys.* **2016**, *12*, 1139–1145. [[CrossRef](#)]
3. Zhang, Z.; Zhang, Y.; Sheng, J.; Yang, L.; Miri, M.-A.; Christodoulides, D.N.; He, B.; Zhang, Y.; Xiao, M. Observation of Parity-Time Symmetry in Optically Induced Atomic Lattices. *Phys. Rev. Lett.* **2016**, *117*, 123601. [[CrossRef](#)]
4. Kang, M.; Chen, J.; Chong, Y.D. Chiral exceptional points in metasurfaces. *Phys. Rev. A* **2016**, *94*, 033834. [[CrossRef](#)]
5. Kang, M.; Liu, F.; Li, J. Effective spontaneous PT-symmetry breaking in hybridized metamaterials. *Phys. Rev. A* **2013**, *87*, 053824. [[CrossRef](#)]
6. Ding, K.; Ma, G.; Xiao, M.; Zhang, Z.Q.; Chan, C.T. Emergence, Coalescence, and Topological Properties of Multiple Exceptional Points and Their Experimental Realization. *Phys. Rev. X* **2016**, *6*, 021007. [[CrossRef](#)]
7. Fleury, R.; Sounas, D.; Alù, A. An invisible acoustic sensor based on parity-time symmetry. *Nat. Commun.* **2015**, *6*, 5905. [[CrossRef](#)]
8. Zhu, X.; Ramezani, H.; Shi, C.; Zhu, J.; Zhang, X. PT-Symmetric Acoustics. *Phys. Rev. X* **2014**, *4*, 031042. [[CrossRef](#)]
9. Ding, K.; Ma, G.; Zhang, Z.Q.; Chan, C.T. Experimental Demonstration of an Anisotropic Exceptional Point. *Phys. Rev. Lett.* **2018**, *121*, 085702. [[CrossRef](#)]
10. Schindler, J.; Li, A.; Zheng, M.C.; Ellis, F.M.; Kottos, T. Experimental study of active LRC circuits with PT symmetries. *Phys. Rev. A* **2011**, *84*, 040101. [[CrossRef](#)]
11. Choi, Y.; Hahn, C.; Yoon, J.W.; Song, S.H. Observation of an anti-PT-symmetric exceptional point and energy-difference conserving dynamics in electrical circuit resonators. *Nat. Commun.* **2018**, *9*, 2182. [[CrossRef](#)] [[PubMed](#)]
12. Assaworarith, S.; Yu, X.; Fan, S. Robust wireless power transfer using a nonlinear parity–time-symmetric circuit. *Nature* **2017**, *546*, 387–390. [[CrossRef](#)]
13. Zhou, J.; Zhang, B.; Xiao, W.; Qiu, D.; Chen, Y. Nonlinear Parity-Time-Symmetric Model for Constant Efficiency Wireless Power Transfer: Application to a Drone-in-Flight Wireless Charging Platform. *IEEE Trans. Ind. Electron.* **2018**, *66*, 4097–4107. [[CrossRef](#)]
14. Zeng, C.; Sun, Y.; Li, G.; Li, Y.; Jiang, H.; Yang, Y.; Chen, H. High-Order Parity-Time Symmetric Model for Stable Three-Coil Wireless Power Transfer. *Phys. Rev. Appl.* **2020**, *13*, 034054. [[CrossRef](#)]
15. Song, J.; Yang, F.; Guo, Z.; Wu, X.; Zhu, K.; Jiang, J.; Sun, Y.; Li, Y.; Jiang, H.; Chen, H. Wireless Power Transfer via Topological Modes in Dimer Chains. *Phys. Rev. Appl.* **2021**, *15*, 014009. [[CrossRef](#)]

16. Yuan, H.Y.; Yan, P.; Zheng, S.; He, Q.Y.; Xia, K.; Yung, M.-H. Steady Bell State Generation via Magnon-Photon Coupling. *Phys. Rev. Lett.* **2020**, *124*, 053602. [[CrossRef](#)] [[PubMed](#)]
17. Lin, Z.; Ramezani, H.; Eichelkraut, T.; Kottos, T.; Cao, H.; Christodoulides, D.N. Unidirectional Invisibility Induced by PT-Symmetric Periodic Structures. *Phys. Rev. Lett.* **2011**, *106*, 213901. [[CrossRef](#)] [[PubMed](#)]
18. Yin, X.; Zhang, X. Unidirectional light propagation at exceptional points. *Nat. Mater.* **2013**, *12*, 175–177. [[CrossRef](#)]
19. Fan, S.; Baets, R.; Petrov, A.; Yu, Z.; Joannopoulos, J.D.; Freude, W.; Melloni, A.; Popović, M.; Vanwolleghem, M.; Jalas, D.; et al. Comment on “Nonreciprocal Light Propagation in a Silicon Photonic Circuit”. *Science* **2012**, *335*, 38. [[CrossRef](#)]
20. Ramezani, H.; Kottos, T.; El-Ganainy, R.; Christodoulides, D.N. Unidirectional nonlinear PT-symmetric optical structures. *Phys. Rev. A* **2010**, *82*, 043803. [[CrossRef](#)]
21. Sukhorukov, A.A.; Xu, Z.; Kivshar, Y.S. Nonlinear suppression of time reversals in PT-symmetric optical couplers. *Phys. Rev. A* **2010**, *82*, 043818. [[CrossRef](#)]
22. Chong, Y.D.; Ge, L.; Stone, A.D. PT-Symmetry Breaking and Laser-Absorber Modes in Optical Scattering Systems. *Phys. Rev. Lett.* **2011**, *106*, 093902. [[CrossRef](#)]
23. Gao, Z.; Fryslie, S.T.M.; Thompson, B.J.; Carney, P.S.; Choquette, K.D. Parity-time symmetry in coherently coupled vertical cavity laser arrays. *Optica* **2017**, *4*, 323–329. [[CrossRef](#)]
24. Longhi, S. PT-symmetric laser absorber. *Phys. Rev. A* **2010**, *82*, 031801. [[CrossRef](#)]
25. Sun, Y.; Tan, W.; Li, H.-Q.; Li, J.; Chen, H. Experimental Demonstration of a Coherent Perfect Absorber with PT Phase Transition. *Phys. Rev. Lett.* **2014**, *112*, 143903. [[CrossRef](#)] [[PubMed](#)]
26. Zeng, C.; Zhu, K.; Sun, Y.; Li, G.; Guo, Z.; Jiang, J.; Li, Y.; Jiang, H.; Yang, Y.; Chen, H. Ultra-sensitive passive wireless sensor exploiting high-order exceptional point for weakly coupling detection. *N. J. Phys.* **2021**, *23*, 063008. [[CrossRef](#)]
27. Zeng, C.; Sun, Y.; Li, G.; Li, Y.; Jiang, H.; Yang, Y.; Chen, H. Enhanced sensitivity at high-order exceptional points in a passive wireless sensing system. *Opt. Express* **2019**, *27*, 27562–27572. [[CrossRef](#)]
28. El-Ganainy, R.; Makris, K.G.; Khajavikhan, M.; Musslimani, Z.H.; Rotter, S.; Christodoulides, D.N. Non-Hermitian physics and PT symmetry. *Nat. Phys.* **2018**, *14*, 11–19. [[CrossRef](#)]
29. Sakhdari, M.; Hajizadegan, M.; Zhong, Q.; Christodoulides, D.N.; El-Ganainy, R.; Chen, P.-Y. Experimental Observation of PT Symmetry Breaking near Divergent Exceptional Points. *Phys. Rev. Lett.* **2019**, *123*, 193901. [[CrossRef](#)]
30. Müller, M.; Rotter, I. Exceptional points in open quantum systems. *J. Phys. A: Math. Theor.* **2008**, *41*, 244018. [[CrossRef](#)]
31. Heiss, W.D. The physics of exceptional points. *J. Phys. A Math. Theor.* **2012**, *45*, 444016. [[CrossRef](#)]
32. Miri, M.-A.; Alù, A. Exceptional points in optics and photonics. *Science* **2019**, *363*, eaar7709. [[CrossRef](#)] [[PubMed](#)]
33. Peng, B.; Özdemir, Ş.K.; Liertzer, M.; Chen, W.; Kramer, J.; Yilmaz, H.; Wiersig, J.; Rotter, S.; Yang, L. Chiral modes and directional lasing at exceptional points. *Proc. Natl. Acad. Sci. USA* **2016**, *113*, 6845–6850. [[CrossRef](#)]
34. Dembowski, C.; Dietz, B.; Gräf, H.-D.; Harney, H.L.; Heine, A.; Heiss, W.D.; Richter, A. Observation of a Chiral State in a Microwave Cavity. *Phys. Rev. Lett.* **2003**, *90*, 034101. [[CrossRef](#)]
35. Tesla, N. Apparatus for Transmitting Electrical Energy. U.S. Patent 1,119,732, 1 December 1914.
36. Kurs, A.; Karalis, A.; Moffatt, R.; Joannopoulos, J.D.; Fisher, P.; Soljačić, M. Wireless Power Transfer via Strongly Coupled Magnetic Resonances. *Science* **2007**, *317*, 83–86. [[CrossRef](#)] [[PubMed](#)]
37. Lerosey, G. Wireless power on the move. *Nature* **2017**, *546*, 354–355. [[CrossRef](#)]
38. Kim, S.; Ho, J.; Poon, A.S.Y. Midfield Wireless Powering of Subwavelength Autonomous Devices. *Phys. Rev. Lett.* **2013**, *110*, 203905. [[CrossRef](#)]
39. Agarwal, K.; Jegadeesan, R.; Guo, Y.-X.; Thakor, N.V. Wireless Power Transfer Strategies for Implantable Bioelectronics. *IEEE Rev. Biomed. Eng.* **2017**, *10*, 136–161. [[CrossRef](#)]
40. Sun, G.; Muneer, B.; Li, Y.; Zhu, Q. Ultracompact Implantable Design With Integrated Wireless Power Transfer and RF Transmission Capabilities. *IEEE Trans. Biomed. Circuits Syst.* **2018**, *12*, 281–291. [[CrossRef](#)]
41. Bocan, K.N.; Mickle, M.H.; Sejdic, E. Tissue Variability and Antennas for Power Transfer to Wireless Implantable Medical Devices. *IEEE J. Transl. Eng. Health Med.* **2017**, *5*, 2700. [[CrossRef](#)] [[PubMed](#)]
42. Khan, S.R.; Pavuluri, S.K.; Cummins, G.; Desmulliez, M.P.Y. Wireless Power Transfer Techniques for Implantable Medical Devices: A Review. *Sensors* **2020**, *20*, 3487. [[CrossRef](#)] [[PubMed](#)]
43. Liang, C.; Zhang, Y.; Li, Z.; Yuan, F.; Yang, G.; Song, K. Coil Positioning for Wireless Power Transfer System of Automatic Guided Vehicle Based on Magnetic Sensing. *Sensors* **2020**, *20*, 5304. [[CrossRef](#)] [[PubMed](#)]
44. Wang, S.; Jiang, C.; Tao, X.; Chen, F.; Rong, C.; Lu, C.; Zeng, Y.; Liu, X.; Liu, R.; Wei, B.; et al. Enhancing the Stability of Medium Range and Misalignment Wireless Power Transfer System by Negative Magnetic Metamaterials. *Materials* **2020**, *13*, 5695. [[CrossRef](#)] [[PubMed](#)]
45. Wang, B.; Teo, K.H.; Nishino, T.; Yerazunis, W.; Barnwell, J.; Zhang, J. Experiments on wireless power transfer with metamaterials. *Appl. Phys. Lett.* **2011**, *98*, 254101. [[CrossRef](#)]
46. Urzhumov, Y.; Smith, D.R. Metamaterial-enhanced coupling between magnetic dipoles for efficient wireless power transfer. *Phys. Rev. B* **2011**, *83*, 205114. [[CrossRef](#)]
47. Song, M.; Smirnov, P.; Puhtina, E.; Zanganeh, E.; Glybovski, S.; Belov, P.; Kapitanova, P. Multi-mode metamaterial-inspired resonator for near-field wireless power transfer. *Appl. Phys. Lett.* **2020**, *117*, 083501. [[CrossRef](#)]

48. Markvart, A.; Song, M.; Glybovski, S.; Belov, P.; Simovski, C.; Kapitanova, P. Metasurface for Near-Field Wireless Power Transfer With Reduced Electric Field Leakage. *IEEE Access* **2020**, *8*, 40224–40231. [[CrossRef](#)]
49. Xie, Y.; Zhang, Z.; Lin, Y.; Feng, T.; Xu, Y. Magnetic Quasi-Bound State in the Continuum for Wireless Power Transfer. *Phys. Rev. Appl.* **2021**, *15*, 044024. [[CrossRef](#)]
50. Huang, T.; Wang, B.; Zhang, W.; Zhao, C. Ultracompact Energy Transfer in Anapole-based Metachains. *Nano Lett.* **2021**, *21*, 6102–6110. [[CrossRef](#)]
51. Badowich, C.; Markley, L. Idle Power Loss Suppression in Magnetic Resonance Coupling Wireless Power Transfer. *IEEE Trans. Ind. Electron.* **2018**, *65*, 8605–8612. [[CrossRef](#)]
52. Zhang, L.; Yang, Y.; Jiang, Z.; Chen, Q.; Yan, Q.; Wu, Z.; Zhang, B.; Huangfu, J.; Chen, H. Demonstration of topological wireless power transfer. *Sci. Bull.* **2021**, *66*, 974–980. [[CrossRef](#)] [[PubMed](#)]
53. Li, Y.; Wang, M.; Zhang, W.; Zhao, M.; Liu, J. A Frequency Locking Method for ICPT System Based on LCC/S Compensation Topology. *Energies* **2019**, *12*, 2626. [[CrossRef](#)]

**Disclaimer/Publisher’s Note:** The statements, opinions and data contained in all publications are solely those of the individual author(s) and contributor(s) and not of MDPI and/or the editor(s). MDPI and/or the editor(s) disclaim responsibility for any injury to people or property resulting from any ideas, methods, instructions or products referred to in the content.